Synthetic Lethal Interaction with BCL-XL Blockade Deepens Response to Cetuximab in Patient-Derived Models of Metastatic Colorectal Cancer

Simonetta M. Leto[1], Martina Ferri[1,2], Francesco Sassi[1], Eugenia R. Zanella[1], Francesca Cottino[1], Valentina Vurchio[1,2], Irene Catalano[1], Alessandro Ferrero[3], Caterina C. Zingaretti[3], Caterina Marchiò[1,4], Elena Grassi[1,2], Livio Trusolino[1,2], and Andrea Bertotti[1,2]

ABSTRACT

Purpose: Approximately 20% of patients with RAS wild-type metastatic colorectal cancer (mCRC) experience objective responses to the anti-EGFR antibody cetuximab, but disease eradication is seldom achieved. The extent of tumor shrinkage correlates with long-term outcome. We aimed to find rational combinations that potentiate cetuximab efficacy by disrupting adaptive dependencies on antiapoptotic molecules (BCL2, BCL-XL, MCL1).

Experimental Design: Experiments were conducted in patient-derived xenografts (PDX) and organoids (PDXO). Apoptotic priming was analyzed by BH3 profiling. Proapoptotic and antiapoptotic protein complexes were evaluated by co-immunoprecipitation and electroluminescence sandwich assays. The effect of combination therapies was assessed by caspase activation in PDXOs and by monitoring PDX growth.

Results: A population trial in 314 PDX cohorts, established from as many patients, identified 46 models (14.6%) with appreciable (>50% tumor shrinkage) but incomplete response to cetuximab. From these models, 14 PDXOs were derived. Cetuximab primed cells for apoptosis, but only concomitant blockade of BCL-XL precipitated cell death. Mechanistically, exposure to cetuximab induced upregulation of the proapoptotic protein BIM and its sequestration by BCL-XL. Inhibition of BCL-XL resulted in displacement of BIM, which was not buffered by MCL1 and thereby became competent to induce apoptosis. In five PDX models, combination of cetuximab and a selective BCL-XL inhibitor triggered apoptosis and led to more pronounced tumor regressions and longer time to relapse after treatment discontinuation than cetuximab alone.

Conclusions: In mCRC tumors that respond to cetuximab, antibody treatment confers a synthetic-lethal dependency on BCL-XL. Targeting this dependency unleashes apoptosis and increases the depth of response to cetuximab.

Introduction

Colorectal cancer is the second leading cause of cancer-related deaths worldwide, with a 5-year survival rate of less than 20% in the metastatic setting (1, 2). The introduction of anti-EGFR mAbs (cetuximab and panitumumab) improved survival in patients with inoperable RAS/RAF wild-type metastatic colorectal cancer (mCRC; refs. 3, 4). However, although response rates are clinically meaningful, anti-EGFR therapy only exceptionally leads to disease eradication, and patients ultimately recur (5). The evidence that mCRC tumors almost invariably relapse after an initial response to therapy supports the notion that lingering cells surviving EGFR inhibition provide a reservoir of residual tumor burden from which drug-resistant progressive disease emerges (6). Importantly, the extent of early tumor shrinkage during anti-EGFR treatment correlates with long-term outcome (7, 8), suggesting that the absolute number of surviving cells directly impacts the risk of relapse. As a consequence, patients with mCRC would likely benefit from therapeutic approaches that increase the depth of response to EGFR blockade, thus shrinking the pool of residual cancer cells. Biologically, the closest analogy to clinical residual disease is the drug-tolerant (or "persister") state (9). Hallmarks of drug-tolerant cells include nongenetic mechanisms of persistence (whereby cells tend to dynamically regain drug sensitivity after a washout period), a slow-cycling phenotype (which may facilitate resilience to stressful conditions) and, notably, reduced propensity to undergo apoptosis (9–11).

Apoptosis is a form of programmed cell death that is regulated at the mitochondrial level by the balance between antiapoptotic proteins (including BCL2, BCL-XL, and MCL1) and proapoptotic activators (including BIM, BID, and PUMA). Upon specific stimuli, proapoptotic activators induce the oligomerization of pore-forming effectors (namely, BAX and BAK), resulting in mitochondrial outer membrane permeabilization (MOMP) and mitochondrial release of apoptogenic molecules like cytochrome c, with subsequent caspase activation and cell death (12). While antiapoptotic proteins contain many BCL2 homology (BH) domains, proapoptotic activators are called "BH3 only" because of their shared homology solely in the BH3 domain, through which they selectively bind to (and are kept at bay by) different antiapoptotic proteins (13). These peculiarities have been leveraged to design a new class of small molecules called BH3 mimetics, which mimic the activity of selected proapoptotic proteins and thus can sensitize cells to mitochondrial apoptosis (14).

The introduction of BH3 mimetics in clinical practice has profoundly changed the treatment of some hematologic malignancies. For

[1]Candiolo Cancer Institute – FPO IRCCS, Candiolo, Torino, Italy. [2]Department of Oncology, University of Torino, Candiolo, Torino, Italy. [3]Mauriziano Umberto I Hospital, Torino, Italy. [4]Department of Medical Sciences, University of Torino, Candiolo, Torino, Italy.

A. Bertotti and L. Trusolino contributed as co-supervisors to this article.

Corresponding Author: Livio Trusolino, Laboratory of Translational Cancer Medicine, Candiolo Cancer Institute—FPO IRCCS, Strada Provinciale 142, km 3.95, Candiolo 10060, Torino, Italy. Phone: 3901-1993-3227; E-mail: livio.trusolino@ircc.it

Clin Cancer Res 2023;29:1102–13

doi: 10.1158/1078-0432.CCR-22-2550

This open access article is distributed under the Creative Commons Attribution-NonCommercial-NoDerivatives 4.0 International (CC BY-NC-ND 4.0) license.

©2023 The Authors; Published by the American Association for Cancer Research

Downloaded from http://aacrjournals.org/clincancerres/article-pdf/29/6/1102/3281404/1102.pdf by guest on 07 April 2023

Translational Relevance

The anti-EGFR antibody cetuximab exerts cytostatic rather than cytotoxic effects in preclinical models of colorectal cancer. This may explain why complete tumor regressions are exceptional events in responsive patients. We report that treatment of metastatic colorectal cancer (mCRC) organoids with cetuximab reduced the apoptotic threshold, but concomitant and selective targeting of BCL-XL was necessary to induce cell death. In patient-derived xenograft models with partial response to single-agent cetuximab, combined inhibition of EGFR and BCL-XL induced deeper tumor shrinkage, minimized cancer cell density, and delayed relapse after treatment withdrawal. Clinical development of the BCL2/BCL-XL inhibitor navitoclax has recently gained momentum thanks to its demonstrated efficacy in improving overall survival in patients with myelofibrosis, and efforts are ongoing to develop last-generation, selective BCL-XL inhibitors. Our findings provide a rationale for clinical investigation of combined EGFR and BCL-XL blockade to increase the magnitude of response in patients with mCRC treated with anti-EGFR antibodies, with potential consequences on progression-free survival.

example, the selective BCL2-inhibitor venetoclax (ABT-199) has been approved for use in chronic lymphocytic leukemia and acute myeloid leukemia on the basis of its excellent clinical activity (15, 16). In patients with solid tumors, BH3 mimetics are usually ineffective as monotherapies (17). However, several preclinical studies have encouraged their use to exacerbate apoptosis in combination with oncogenic kinase small-molecule inhibitors in contexts where the effect of single-agent therapy with kinase inhibitors is limited to proliferation arrest (11, 18–24).

Previous work from our group has shown that the effect of cetuximab in mCRC patient-derived models is cytostatic rather than cytotoxic (10, 25). Here, we hypothesized that the inability of cetuximab to induce overt cell death could be explained by a mechanism of antiapoptotic adaptation, and we reasoned that the identification of specific antiapoptotic dependencies triggered by EGFR blockade could be exploited to convert the growth-inhibitory effect of cetuximab into a fully apoptotic outcome. Using a collection of mCRC patient-derived xenografts (PDX) and organoids (PDXO), we found that EGFR blockade made tumors universally dependent on BCL-XL to evade apoptosis. The combination of cetuximab with BH3 mimetics targeting BCL-XL unleashed apoptosis in organoids and minimized residual disease *in vivo*. These results motivate designing rational therapeutic strategies that may reduce the pool of residual cells in response to anti-EGFR therapies and delay disease recurrence in patients with mCRC.

Materials and Methods

PDXO cultures

Organoids were established from PDX explants. Tumor specimens (0.5 cm × 0.5 cm) were chopped with a scalpel and washed with PBS. After centrifugation, the final cell preparation was embedded in Matrigel (Corning) or Cultrex Basement Membrane Extract (BME, R&D Systems) and dispensed onto 24-well plates (Corning). After 10–20 minutes at 37°C, culture medium was added. Complete mCRC organoid medium composition is the following: DMEM/F12 supplemented with penicillin-streptomycin, 2 mmol/L L-glutamine, 1 mmol/L n-Acetyl Cysteine, B27 (Thermo Fisher Scientific), N2 (Thermo Fisher Scientific), and 20 ng/mL EGF (Sigma-Aldrich). Organoids were tested for *Mycoplasma* and maintained at 37°C in a humidified atmosphere of 5% CO_2.

Dynamic BH3 profiling

Buffers and procedures for FACS-based dynamic BH3 profiling experiments were based on protocols described by the Letai Lab (https://letailab.dana-farber.org/bh3-profiling.html; ref. 26) and optimized for organoid cultures. Briefly, PDXOs were either left untreated or pretreated with cetuximab (20 μg/mL) for 24 hours; then, organoids were gently washed with PBS, incubated with trypsin-EDTA solution (Sigma-Aldrich) for 5 minutes at 37°C, and vigorously pipetted to obtain a single-cell suspension. To distinguish live versus dead cells, viability staining was performed using the Zombie Aqua fluorescent dye (BioLegend). Cells were then suspended in MEB buffer (26) to the final concentration of 2×10^6 cells/mL and 50 μL of cell suspension were added to each well of a 96-well plate (Corning). BH3 peptides (New England Peptide) at twice their final concentration in MEB plus 0.002% digitonin were preadded to each well (50 μL/well). The plate was incubated at 25°C for 60 minutes in the INCU-Line incubator (VWR International) followed by the addition of 33 μL 4% formaldehyde in PBS for 10 minutes at room temperature. Fixation was terminated by the addition of 33 μL buffer N2 (26) for at least 5 minutes. Cytochrome c staining was performed by adding 20 μL of a 1:40 dilution of anti-cytochrome c antibody (BioLegend) in BD Perm/Wash Buffer overnight at 4°C. The inert peptide PUMA2A (100 μmol/L) was used as a control for full cytochrome c retention and alamethicin (25 μmol/L), which causes BAX/BAK-independent MOMP, was used as control for full cytochrome c release. During FACS analysis, gating around the cells exposed to PUMA2A using side scatter versus cytochrome c provided the percentage of cytochrome c positive cells, and 100 minus this value defined the percentage of cytochrome c loss.

Viability and apoptosis assays

Pharmacologic experiments were performed in 96-well plates with a thin layer of BME in each well. PDXOs were washed with PBS, incubated with trypsin-EDTA solution for 5 minutes at 37°C, and vigorously pipetted to obtain a single-cell suspension. Cells were seeded in 2% BME culture medium at the confluence of 5,000 cells/well in the absence of EGF. After 1–2 days from seeding, PDXOs were treated with the modalities indicated in the figure legends. Navitoclax and venetoclax were purchased from Chemgood. Cell viability and apoptotic activity were measured using the Cell Titer-Glo and Caspase-Glo 3/7 luminescent assay kits (Promega), respectively. In the presented heatmaps, signals were normalized to the sum of the values of the corresponding experiments and reported as a fraction of the maximum value.

Immunoprecipitation and immunoblot analyses

Proteins were extracted with cold EB buffer (50 mmol/L Hepes pH 7.4, 150 mmol/L NaCl, 1% Triton X-100, 10% glycerol, 5 mmol/L EDTA, 5 mmol/L EGTA) in the presence of phosphatase and protease inhibitors (Thermo Fisher Scientific). Immunoprecipitations were performed by incubating protein extracts with either the anti-BCL-XL or the anti-MCL1 primary antibody and Protein A sepharose beads (GE Healthcare) for 1 hour at 4°C. Immunoprecipitated or total proteins were electrophoresed on precast polyacrylamide gels (Invitrogen) and transferred onto nitrocellulose membranes using a Trans-Blot Turbo Blotting System (Bio-Rad).

Downloaded from http://aacrjournals.org/clincancerres/article-pdf/29/6/1102/3281404/1102.pdf by guest on 07 April 2023

Membrane-bound antibodies were detected by the enhanced chemiluminescence system (Promega). Primary antibodies were the following: rabbit anti-BCL2 (Abcam, #ab32124), rabbit anti-BCL-XL (Cell Signaling Technology, #2762), rabbit anti-MCL1 (Cell Signaling Technology, #94296), rabbit anti-BIM (Cell Signaling Technology, #2933), and mouse anti-vinculin (Sigma-Aldrich, V9131). BT-474 cells were purchased from ATCC and used as controls for protein expression.

Meso Scale Discovery assays

BIM:BCL-X (BCL-XL and BCL-XS, long and short isoforms of BCL-X) and BIM:MCL1 complexes were measured by Meso Scale Discovery (MSD) assays (#F218A-3 and #F216Z-3, Meso Scale Diagnostics) according to manufacturer's instructions. MSD GOLD 96-well Small Spot SA SECTOR plates (#L45SA-2) were coated with biotin human BCL-X and MCL1 capture antibodies in independent wells. After incubation with protein extracts, SULFO-TAG human BIM detection antibody (#F218A-3) was used to measure the total amount of BIM:BCL-X and BIM:MCL1 complexes. Results were read using the MSD QuickPlex SQ 120 Reader.

IHC and morphometric analyses

Tumors were formalin fixed, paraffin embedded, and subjected to hematoxylin and eosin staining or IHC analysis with rabbit anti-cleaved caspase-3 (Cell Signaling Technology, #9661) or rabbit anti-BIM antibody (Cell Signaling Technology, #2933). After incubation with secondary antibodies, immunoreactivities were revealed by DAB chromogen (Dako). Images were captured with the Leica LAS EZ software using a Leica DM LB microscope. Morphometric quantitation was performed by ImageJ software using spectral image segmentation. Software outputs were manually verified by visual inspection of digital images.

Real-time qRT-PCR

Total RNA was extracted using the Maxwell Instrument (Promega) and reverse transcribed using High-Capacity cDNA reverse transcription (Life Technologies). Results were normalized to the average of two housekeeper genes (*CETN2* and *HPRT1*). The Taqman probes (Life Technologies) were the following: Hs00608023_m1 (*BCL2*), Hs00236329_m1 (*BCL2L1*/BCL-XL), Hs01050896_m1 (*MCL1*), Hs00708019_s1 (*BCL2L11*/BIM), Hs00942570_g1 (*CETN2*), and Hs02800695_m1 (*HPRT1*).

PDX studies

Tumor implantation and expansion were performed as previously described in 6-week-old male and female NOD/SCID mice (27). Mice with established tumors (average volume ∼400 mm^3) were randomized and treated with the modalities indicated in the figures. A-1331852 was dissolved in 60% Phosal 50 PG, 30% PEG-400, and 10% ethanol. Tumor size was evaluated once weekly by caliper measurements, and the approximate volume of the mass was calculated using the formula $4/3\pi \cdot (d/2)^2 \cdot D/2$, where d is the minor tumor axis and D is the major tumor axis. Results were considered interpretable when a minimum of 5 mice per treatment group reached the prespecified endpoints (at least 3 weeks on therapy or development of tumors with average volumes larger than 600 mm^3 within each treatment group in trials aimed to assess drug efficacy; at least 3 weeks after treatment cessation or development of individual tumors with volumes larger than 750 mm^3 in survival experiments aimed to assess tumor control by therapy). All values for tumor growth curves were recorded blindly. *In vivo* procedures and related biobanking data were managed using the Laboratory Assistant Suite (28). Animal procedures were approved by the Italian Ministry of Health (authorization 806/2016-PR).

Statistical analyses

The number of biological (nontechnical) replicates for each experiment is reported in the figure legends. For experiments with two groups, statistical analysis was performed using two-tailed Welch *t* test. For experiments with more than two groups, one-way ANOVA was used. In case of multiple testing, we adopted the Šidák correction for multiple comparisons. Correlations were calculated by Spearman coefficients. Statistical analyses in the survival experiments were performed by log-rank (Mantel–Cox) test. The level of statistical significance was set at $P < 0.05$. Graphs were generated and statistical analyses were performed using the GraphPad Prism (v9.0) statistical package.

Data availability

The raw data generated in this study are available upon request from the corresponding author.

Results

EGFR blockade increases apoptotic priming and BIM:BCL-XL interaction

For selection of models that could benefit from combinatorial therapies aimed to increase the depth of response to EGFR inhibition, we evaluated the population-level distribution of tumor response to single-agent cetuximab in a collection of 314 mCRC PDXs, established from as many patients, part of which had been used in previous studies (10, 25, 27, 29, 30). Only 46 models (14.6%) experienced at least 50% mean tumor volume reduction after 3 weeks of cetuximab (**Fig. 1A**), indicating that the paucity of massive regressions observed in the clinic was recapitulated in PDXs. All cetuximab-sensitive models did not harbor resistance-driving mutations in *KRAS*, *NRAS,* and *BRAF* genes, again in accordance with clinical reality (ref. 5; **Fig.1A**). From 14 cetuximab-responsive models, randomly selected, we generated PDXOs for preclinical experimentation *in vitro* (**Fig. 1A**, green bars).

Several studies have demonstrated the biological fidelity of PDOs in preserving the fundamental characteristics of parental tumors, including concordance in drug responses (31–33). However, little is known whether PDXOs retain the drug sensitivity profiles of their matched PDXs. As a proof of concept, we compared the effects of cetuximab on PDXO viability with tumor volume changes after antibody treatment in the corresponding PDXs of origin. In line with *in vivo* responses, PDXOs proved to be sensitive to EGFR blockade and displayed a high correlation with their matched *in vivo* counterparts in the extent of growth inhibition (**Fig. 1B**). This attests to the reliability of our PDXO models as surrogates of PDXs for *in vitro* studies.

To explore whether cetuximab treatment influences the propensity of mCRC cells to undergo apoptosis (a property named "apoptotic priming"), we deployed a functional assay called dynamic BH3 profiling (26, 34). Specifically, we measured the percentage of cytochrome c release from mitochondria after cell exposure to synthetic BH3 peptides (binding antiapoptotic molecules) in 10 PDXOs treated with vehicle or cetuximab for 24 hours. As previously reported for PDX-isolated cultures of triple-negative breast cancer (35), we considered a threshold difference of 10% in the magnitude of cytochrome c mobilization between drug-treated

Downloaded from http://aacrjournals.org/clincancerres/article-pdf/29/6/1102/3281404/1102.pdf by guest on 07 April 2023

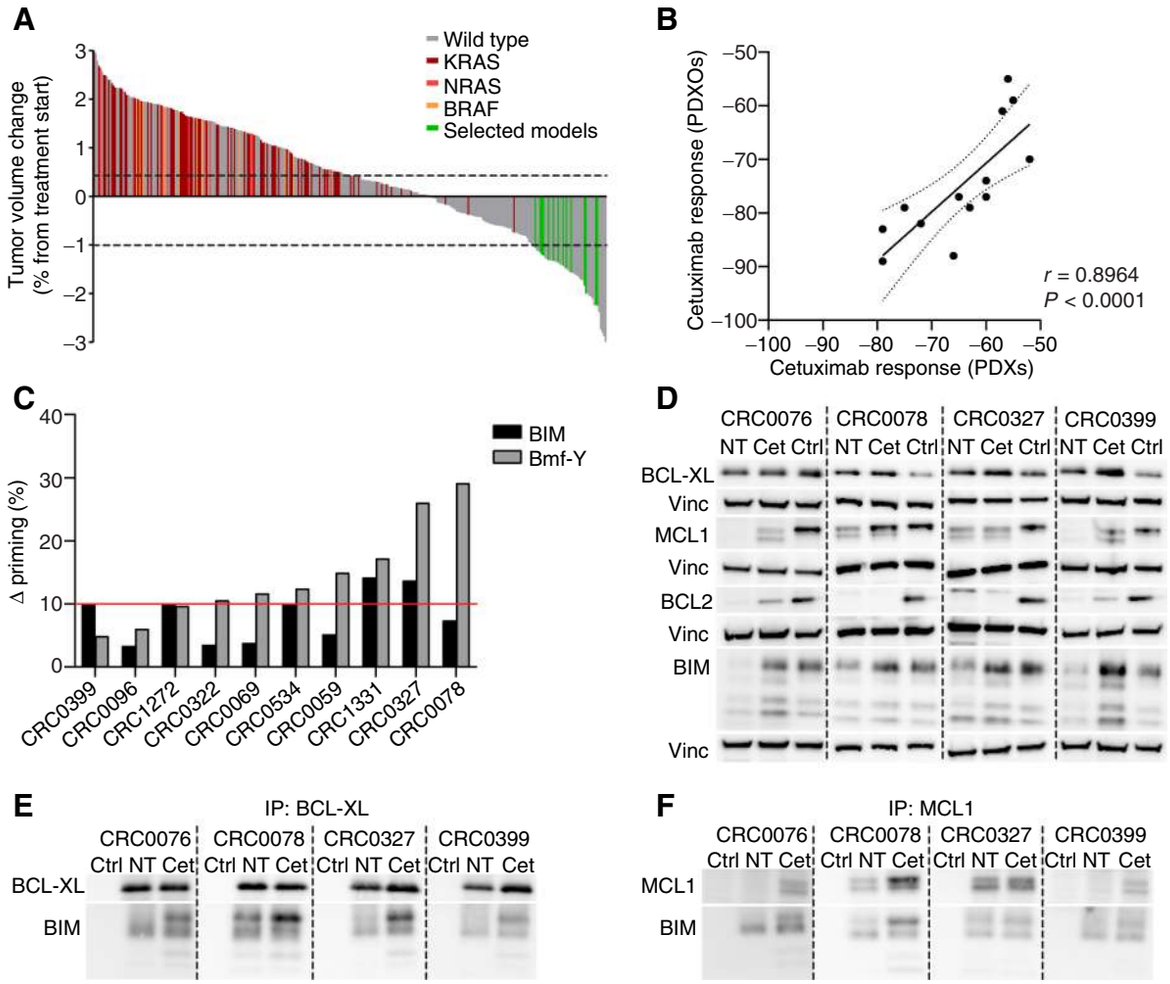

Figure 1.

EGFR blockade increases apoptotic priming and induces preferential binding of upregulated BIM to BCL-XL. **A,** Cetuximab response after 3 weeks of treatment (20 mg/kg, intraperitoneal injection twice a week) compared with tumor volume the day before treatment initiation in 314 mCRC PDX models ($n = 6$ or 12 mice for each bar, depending on whether initial engraftment was successful in 1 or 2 mice). Response categories were arbitrarily defined: regression (below the lower dotted line, −50%); progressive disease (above the upper dotted line, +35%); and disease stabilization (between the dotted lines). Wild-type denotes cases with no mutations in *KRAS*, *NRAS*, or *BRAF*. Selected models denotes cases from which PDXOs were generated. **B,** Scatter plot showing simple linear regression of cetuximab response profiles in 13 selected PDXOs (percentage of cell viability reduction relative to untreated controls) and in their corresponding PDXs of origin (percentage of tumor volume variation after 3 weeks of treatment compared with tumor volume the day before treatment initiation). Organoids were treated with cetuximab (20 μg/mL) for 1 week, then cell viability was assessed by ATP content (Cell Titer Glo assay). PDXs were treated with cetuximab as described in **A**. Dotted lines indicate the 95% confidence bands of the best-fit line. Statistical analysis by Spearman correlation coefficient. **C,** Delta priming response to BIM (0.003 μmol/L) and Bmf-Y (1 μmol/L) peptides in 10 PDXOs after cetuximab treatment (24 hours, 20 μg/mL). Delta priming = % cytochrome c loss^{cetuximab} − % cytochrome c loss^{untreated}. Each bar represents the average of two independent experiments or, for CRC0078, a single experiment. Western blot analysis with the indicated antibodies in whole-cell extracts (**D**) or after immunoprecipitation with antibodies agains BCL-XL (**E**) or MCL1 (**F**) in four PDXOs. Organoids were treated with 20 μg/mL cetuximab for 72 hours. NT, untreated control; Cet, cetuximab; Vinc, vinculin (loading control); Ctrl, BT-474 cell extracts as a positive control for antibody specificity (**D**) or beads without capture antibody as a negative control for immunoprecipitates (**E** and **F**). Images from a second experiment on independent biological replicates are shown in Supplementary Fig. S1.

cells and untreated controls ("delta priming") as a biologically relevant indicator of apoptotic sensitization induced by therapy. Post-cetuximab delta priming was increased to near- or above-threshold levels after exposure to the promiscuous Bmf-Y or BIM peptides in eight and five PDXOs, respectively; only one model (CRC0096) was poorly primed by cetuximab (**Fig. 1C**). These results indicate that EGFR blockade overall enhances the apoptotic predisposition of colorectal cancer tumors, thus rendering them more susceptible to proapoptotic insults.

To investigate the molecular bases of cetuximab-induced apoptotic priming, we examined the effect of EGFR inhibition on the stoichiometry of the most relevant apoptosis regulators (the antiapoptotic molecules BCL2, BCL-XL, and MCL1, and the proapoptotic molecule BIM) in four PDXO models. BCL-XL protein expression was not changed after a 72-hour treatment with cetuximab (**Fig. 1D**; Supplementary Fig. S1A). At variance, MCL1 levels were inconsistently modulated by treatment across models and even among different experimental replicates of the same case. In particular, after cetuximab

Downloaded from http://aacrjournals.org/clincancerres/article-pdf/29/6/1102/3281404/1102.pdf by guest on 07 April 2023

treatment, MCL1 protein quantities were either stable or downregulated in one model (CRC0327) and either stable or upregulated in the remaining three cases (**Fig. 1D**; Supplementary Fig. S1A). This variability may be related to the high instability of MCL1 protein levels (36). BCL2 protein expression was overall negligible and was not affected by cetuximab treatment (**Fig. 1D**; Supplementary Fig. S1A). Lower expression of BCL2 in comparison with BCL-XL and MCL1 was also observed at the transcriptional level, as evaluated by qRT-PCR in our representative panel of 14 PDXOs (Supplementary Fig. S1B). Notably, EGFR inhibition led to pronounced upregulation of the BIM protein in all models tested (**Fig. 1D**; Supplementary Fig. S1A). This is consistent with prior studies showing that BIM protein turnover is affected by EGFR downstream signals (22, 37, 38).

Next, we evaluated whether cetuximab-induced upregulation of BIM influenced its interaction with BCL-XL and MCL1. Co-immunoprecipitation experiments documented a consistent increase in the extent of BIM interaction with BCL-XL upon cetuximab treatment in the analyzed PDXOs (**Fig. 1E**; Supplementary Fig. S1C). In agreement with the observation that MCL1 expression was variably modulated by EGFR inhibition (**Fig. 1D**; Supplementary Fig. S1A), also the changes of BIM binding to MCL1 after cetuximab did not show a clear pattern. Specifically, MCL1:BIM complexes were reproducibly increased in one model (CRC0076), were either stable or increased in another model (CRC0078), and remained substantially unaffected in the remaining two models (CRC0327 and CRC0399; **Fig. 1F**; Supplementary Fig. S1D). Collectively, these findings suggest that cetuximab-induced apoptotic priming is mediated by upregulation of proapoptotic BIM; however, induction of overt apoptosis is prevented by BIM sequestration by BCL-XL.

Selective BCL-XL inhibition potentiates the therapeutic effect of EGFR blockade by unleashing apoptosis in cetuximab-sensitive organoids

We hypothesized that the preferential binding of upregulated BIM to BCL-XL may render cetuximab-treated cells dependent on BCL-XL to elude cell death and, consequently, more susceptible to BCL-XL inhibition. To test this hypothesis, we treated our entire collection of 14 cetuximab-sensitive PDXO lines with navitoclax (ABT-263), a dual BCL2/BCL-XL inhibitor currently in clinical development, either alone or in combination with cetuximab. After 48 hours of treatment, overall cell numbers were more markedly reduced by combination therapy than by single-agent cetuximab or navitoclax (**Fig. 2A**, top; Supplementary Fig. S2), suggesting that targeting BCL-XL may enhance the therapeutic efficacy of cetuximab alone.

Navitoclax promiscuously inhibits both BCL-XL and BCL2. To rule out any contribution of BCL2 to limiting cetuximab efficacy, we compared the effect of navitoclax with that of selective inhibitors targeting BCL-XL or BCL2. Monotherapy with the selective BCL-XL inhibitor A-1331852 reduced cell proliferation to an extent similar to that achieved with navitoclax (**Fig. 2A**, top; Supplementary Fig. S2), whereas the BCL2 selective inhibitor venetoclax was completely ineffective (**Fig. 2B**; Supplementary Fig. S2). When combined with cetuximab, A-1331852 drastically impaired cell proliferation, mimicking or even outperforming navitoclax (**Fig. 2A**, top; Supplementary Fig. S2). Conversely, the addition of venetoclax did not enhance the effect of cetuximab monotherapy (**Fig. 2B**; Supplementary Fig. S2).

We then analyzed the impact of the same treatment modalities on apoptosis induction. As previously shown in colorectal cancer cell lines (10), cetuximab alone was unable to increase caspase 3/7 activity when compared to untreated controls (**Fig. 2C** and **D**; Supplementary Fig. S2). As monotherapies, both BCL-XL–targeting compounds, but not the BCL2 selective inhibitor, modestly induced caspase 3/7 activation. In contrast, dual EGFR and BCL-XL blockade by concomitant treatment with cetuximab and navitoclax or cetuximab and A-1331852 triggered massive caspase activation in all models tested (**Fig. 2C**, top, and **D**; Supplementary Fig. S2). Notably, the effect of A-1331852 was again stronger than that observed with navitoclax, possibly because of higher binding affinity to BCL-XL and more potent cellular activity (39).

The apoptotic outcome of combined EGFR and BCL-XL blockade was widely distributed across all models, indicating a common biological vulnerability shared by cetuximab-sensitive mCRC tumors. In this context of general susceptibility, we observed a modest but significant correlation between the extent of response to A-1331852 plus cetuximab combination therapy and the ratio of BCL-XL to BIM mRNA expression (Supplementary Fig. S3). In contrast, we did not detect associations between the drug sensitivity profiles and the expression of BCL-XL, MCL1, or the ratio of MCL1 to BIM (Supplementary Fig. S3). This attests to the key role of BCL-XL:BIM complex formation and disruption for apoptosis regulation in colorectal cancer.

Finally, we tested whether models displaying primary resistance to cetuximab could be sensitized to antibody treatment by BCL-XL inhibition. To do so, we generated PDXOs from two *KRAS*, *NRAS,* and *BRAF* wild-type PDXs that had progressed on cetuximab (Supplementary Fig. S4A). We also generated PDXOs from two PDXs harboring *NRAS* Q61K mutations (Supplementary Fig. S4A) as control models with known mechanisms of primary resistance. Lack of response to cetuximab, as observed in PDXs, was recapitulated in the matched PDXOs (Supplementary Fig. S4B). In these cetuximab-resistant organoids, reduction of cell proliferation and increase of caspase 3/7 activity after single-agent treatment with navitoclax or A-1331852 were slightly more pronounced than those observed in cetuximab-sensitive organoids. However, the addition of cetuximab was inconsequential (**Fig. 2A** and **C**, bottom; Supplementary Fig. S2). Consistent with its inability to enhance apoptosis, cetuximab did not induce BIM upregulation in resistant models (Supplementary Fig. S4C). Overall, these results indicate that EGFR inhibition adaptively leads to a selective dependency on BCL-XL that can be exploited therapeutically to unleash apoptosis, but this occurs only in tumors that basally show some intrinsic responsiveness to EGFR blockade.

Combined inhibition of EGFR and BCL-XL favors BIM release from antiapoptotic molecules

To investigate the mechanisms by which combined BCL-XL and EGFR inhibition unleashed apoptosis in mCRC cells, we treated four sensitive PDXO models with cetuximab, either alone or in combination with navitoclax, and assessed BIM binding to BCL-XL or MCL1 using the MSD platform, a technology that enables quantitative analysis of protein associations by electrochemiluminescence detection. Because long-term treatment with combination therapy had a drastic effect on cell viability (**Fig. 2A**, top, and **B**), we limited treatment duration to 8 hours to ensure the recovery of sufficient amounts of cells for MSD analysis. In line with co-immunoprecipitation experiments (**Fig. 1E** and **F**; Supplementary Fig. S1C and D), cetuximab induced the association of BIM and BCL-XL (**Fig. 3A**) but did not prompt the formation of BIM:MCL1 complexes (**Fig. 3B**). Consistent with its mechanism of action, navitoclax impaired the interaction between BIM and BCL-XL, both basally and after cetuximab treament (**Fig. 3A**). In accordance with our observation that the modulation of MCL1 protein abundance was heterogeneous in different experiments and in different organoids, MCL1:BIM complexes displayed larger variability across models than BCL-XL:BIM complexes, with a

Downloaded from http://aacrjournals.org/clincancerres/article-pdf/29/6/1102/3281404/1102.pdf by guest on 07 April 2023

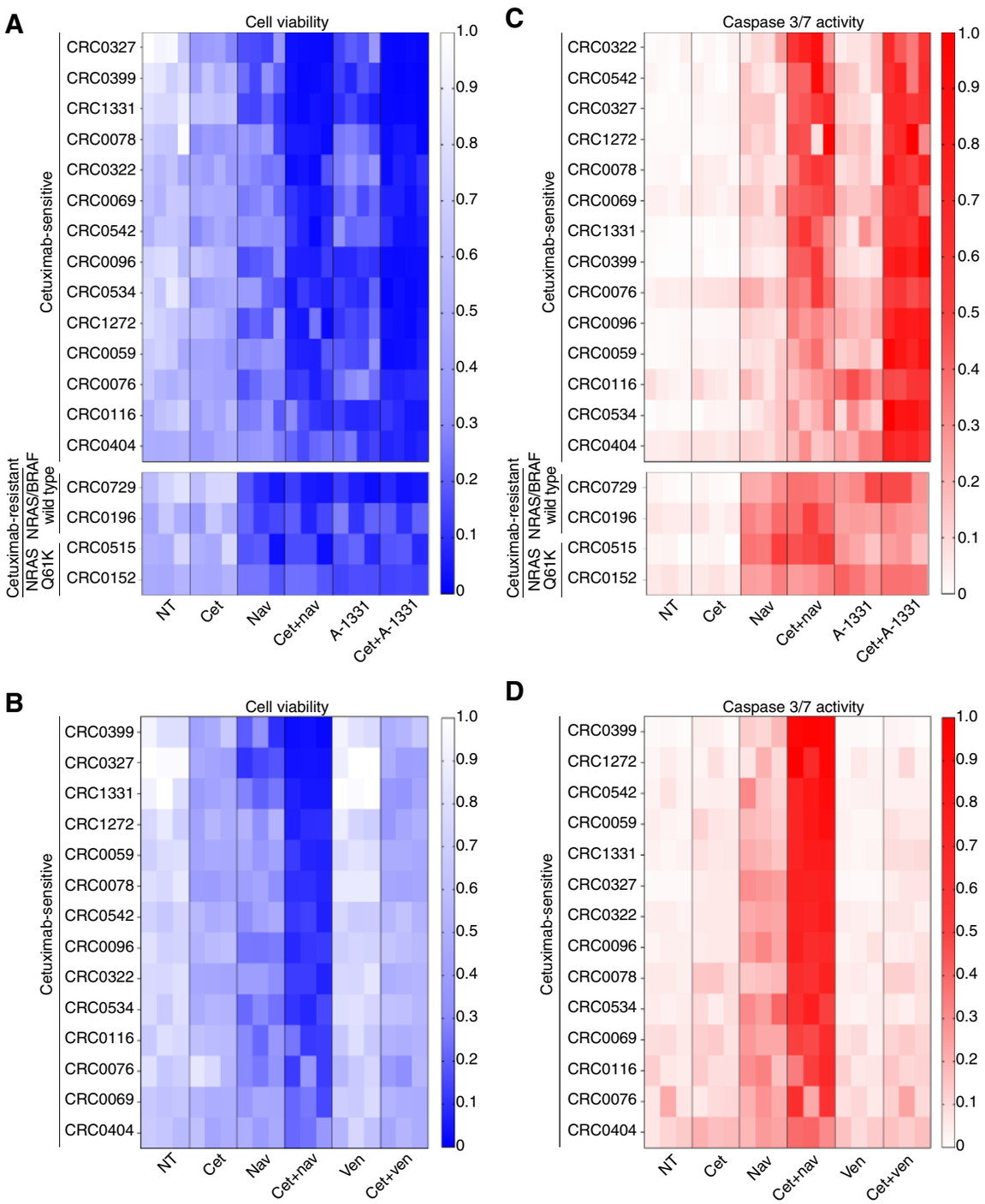

Figure 2.

Selective BCL-XL inhibition potentiates the therapeutic effect of EGFR blockade by unleashing apoptosis in cetuximab-sensitive organoids. Evaluation of cell viability based on ATP content (**A** and **B**) and evaluation of apoptosis based on caspase 3/7 activity (**C** and **D**) in 14 cetuximab-sensitive and four cetuximab-resistant PDXOs treated with the indicated drugs at the following concentrations: cetuximab, 20 μg/mL; navitoclax, 1 μmol/L; A-1331852, 0.5 μmol/L; venetoclax, 1 μmol/L. Organoids were treated for 48 hours in four independent experiments (cetuximab-sensitive PDXOs in **A** and **C**, top) or three independent experiments (cetuximab-resistant PDXOs in **A** and **C**, bottom; all models in **B** and **D**). For each experiment, results are shown as the means of four biological replicates (cetuximab-sensitive PDXOs in **A** and **C**, top) or five biological replicates (cetuximab-resistant PDXOs in **A** and **C**, bottom; all models in **B** and **D**). Caspase 3/7 activity signals were normalized against viable cells, which were treated in parallel with the same modalities and assessed by ATP content. NT, untreated control; Cet, cetuximab; Nav, navitoclax; Ven, venetoclax; A-1331, A-1331852. Results of statistical analysis are reported in Supplementary Fig. S2.

Downloaded from http://aacrjournals.org/clincancerres/article-pdf/29/6/1102/3281404/1102.pdf by guest on 07 April 2023

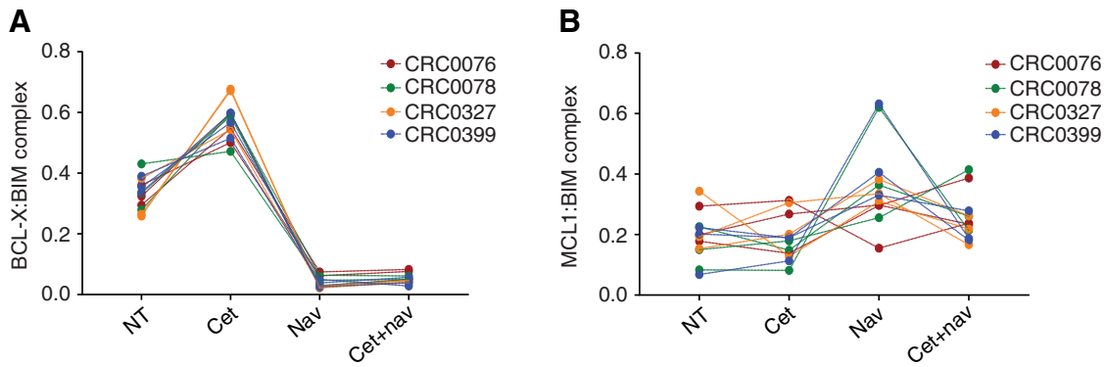

Figure 3.

Dual blockade of EGFR and BCL-XL leads to BIM release from both BCL-XL and MCL1. Four different PDXOs were treated for 8 hours with the indicated drugs and BIM binding to BCL-XL (**A**) or MCL1 (**B**) was quantified by MSD assay. Three independent experiments were performed in each PDXO. For each experiment, signals were normalized against the sum of their values and plotted as individual dots connected by lines. **A,** NT versus Cet, $P < 0.0001$; NT versus Nav, $P < 0.0001$; Cet versus Cet + Nav, $P < 0.0001$. **B,** NT versus Cet, $P > 0.9999$; NT versus Nav, $P = 0.0002$; Cet versus Cet + Nav, $P = 0.3443$; Nav versus Cet + Nav, $P = 0.0248$. Statistical analysis by one-way ANOVA followed by Šidák correction. NT, untreated control; Cet, cetuximab; Nav, navitoclax.

significant overall increase after single-agent navitoclax (**Fig. 3B**). The partial sequestration of BIM by MCL1 after individual BCL-XL inhibition may limit the fraction of BIM available to induce apoptosis, thus explaining the modest response to anti-BCL-XL monotherapies in PDXOs (**Fig. 2A** and **C**, top). Importantly, when cetuximab was combined with navitoclax, displaced BIM was not significantly sequestered by MCL1 (**Fig. 3B**); lack of BIM buffering by MCL-1 after release from BCL-XL likely made the amount of free BIM sufficient to induce overt apoptosis.

Combined EGFR/BCL-XL blockade reduces residual disease *in vivo*

Concomitant blockade of EGFR and BCL-XL triggered stronger apoptosis than either monotherapy *in vitro* (**Fig. 2C**, top, and **D**). Therefore, we assessed whether BCL-XL inhibition could enhance the efficacy of cetuximab also *in vivo*. Because the BCL-XL selective inhibitor A-1331852 elicited similar or even higher proapoptotic effects than navitoclax in PDXOs (**Fig. 2A** and **C**, top), we focused on this agent for further validation in PDXO-matched PDXs.

When used as monotherapy in three cetuximab-sensitive PDX models, A-1331852 did not substantially affect tumor growth (Supplementary Fig. S5), in line with previous studies in human colorectal cancer cell line xenografts showing negligible single-agent activity of BH3 mimetics against BCL-XL (40, 41). We therefore evaluated the efficacy of combination therapy with cetuximab and A-1331852, compared with cetuximab alone, in five cetuximab-sensitive PDXs. As expected, all models exhibited antibody sensitivity after 5 weeks of treatment (**Fig. 4A**). In two cases (CRC0399 and CRC1331), combination therapy was superior over single-agent cetuximab in enhancing tumor shrinkage (**Fig. 4A**). In the remaining three cases (CRC1272, CRC0322, and CRC0059), combination therapy did not significantly outperform cetuximab in reducing tumor size (**Fig. 4A**). However, the regression of CRC0059 after combination therapy was increased by more than 25% when compared with that measured after cetuximab alone (−45.65% after cetuximab monotherapy vs. −71.57% after combination therapy). Of note, the two models in which combination therapy did not further regress palpable masses (CRC1272 and CRC0322) were both extremely sensitive to cetuximab alone (mean tumor volume changes of −95.28% and −89.92%, respectively). We reasoned that this profound response could mask the contribution of A-1331852 (as caliper-based tumor measurements are not precise with very small masses) and decided to quantify histologic cancer cell density as a more reliable readout of tumor burden. Indeed, model CRC1272 showed decreased representation of epithelial neoplastic islets in response to combination therapy compared with single-agent cetuximab (**Fig. 4B**). Likewise, the already drastic reduction of cancer cell density engendered by cetuximab alone in CRC0322 (down to 5.87% of the total tumor area) was further abated to 4.42% by the addition of A-1331852 (**Fig. 4B**). As expected, the deeper tumor shrinkage caused by combination therapy in CRC0059 resulted in lower cancer cell density (**Fig. 4B**). Importantly, the larger extent of microscopic residual disease reduction observed in models in which combination therapy did not induce more pronounced macroscopic regressions invariably translated into longer time to relapse after treatment discontinuation (**Fig. 4C**).

Finally, we analyzed the pharmacodynamic effects of cetuximab alone versus cetuximab plus A-1331852 in the PDX trials. In agreement with findings in PDXOs, single-agent cetuximab only slightly increased the number of apoptotic cells, and only in some models. Conversely, the combination with A-1331852 was consistently accompanied by stronger apoptosis (**Fig. 4D**). BIM protein modulation in PDXs also confirmed results in PDXOs, with all responsive xenografts displaying increased abundance of BIM after cetuximab monotherapy (**Fig. 5**). Interestingly, cetuximab-induced BIM upregulation was maintained also in the presence of A-1331852 (**Fig. 5**), supporting the notion that the higher availability of BIM, together with its displacement from BCL-XL, may lead to the enhanced therapeutic efficacy of combination therapy. In line with that observed in matched PDXOs, antibody treatment did not induce BIM upregulation in cetuximab-resistant PDXs (Supplementary Fig. S6). In summary, dual blockade of EGFR and BCL-XL minimized residual disease in cetuximab-sensitive PDXs by either increasing the depth of macroscopic response or by reducing the number of lingering cancer cells, with positive consequences on tumor control after therapy suspension.

Discussion

Preclinical evidence has shown that mCRC PDXs captured at the moment of maximum shrinkage during cetuximab administration have massive reduction of cancer cell proliferation but do not display

Downloaded from http://aacrjournals.org/clincancerres/article-pdf/29/6/1102/3281404/1102.pdf by guest on 07 April 2023

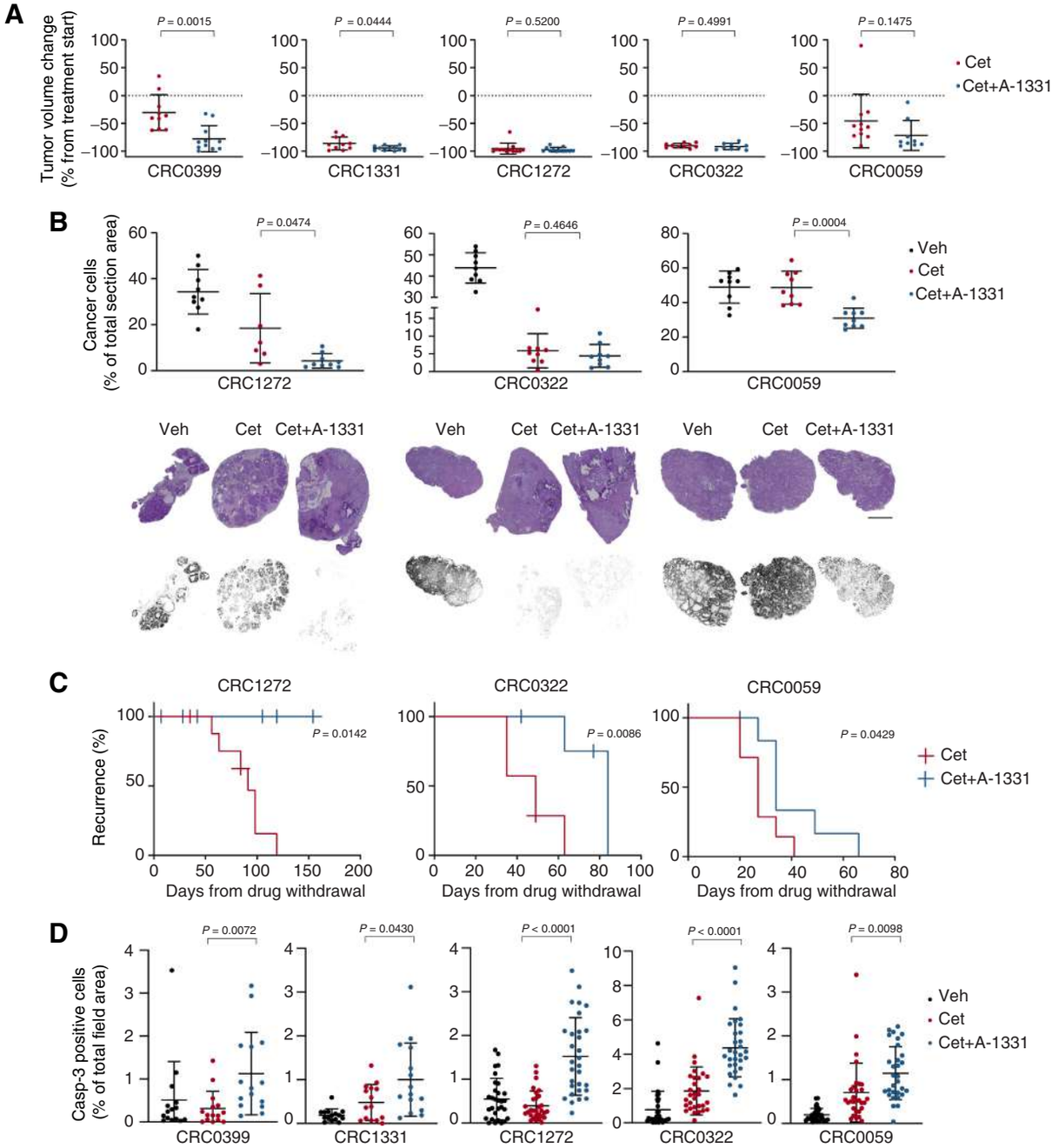

Figure 4.

Combined inhibition of EGFR and BCL-XL unleashes apoptosis and reduces residual disease in mCRC PDXs. **A,** Tumor volume changes in PDXs from mice treated with the indicated modalities for 5 weeks. Cetuximab, 20 mg/kg (intraperitoneal injection twice a week); A-1331852, 25 mg/kg (oral gavage 5 days a week). Dots represent volume changes of PDXs from individual mice, and plots show the means ± SD for each treatment arm. $n = 9$ to 12 animals per each treatment arm. Statistical analysis by two-tailed unpaired t test with Welch correction. **B,** Microscopic assessment of residual cancer cell burden in PDXs treated with the indicated modalities. Top panels indicate morphometric quantifications ($n = 7$ to 9 depending on the extent of section area); bottom panels show hematoxilin and eosin staining and visualization of cancer cells by digital segmentation. Statistical analysis by two-tailed unpaired t test with Welch correction. Scale bar, 500 μm. **C,** Kaplan–Meier survival curves in PDXs following cessation of the indicated treatments. $n = 6$ to 9 animals per each treatment arm. Statistical analysis by log-rank (Mantel–Cox) test. **D,** Morphometric quantification of apoptosis (cleaved caspase 3) in PDXs treated for 24 hours with the indicated modalities. After treatment, three tumors from 3 different mice were explanted and subjected to IHC analysis. Each dot represents the value measured in one optical field (20X), with 5 to 10 optical fields per tumor depending on the extent of section area ($n = 15$–30). The plots show means ± SD. Statistical analysis by two-tailed unpaired t test with Welch correction. Veh, vehicle; Cet, cetuximab; A-1331, A-1331852.

Downloaded from http://aacrjournals.org/clincancerres/article-pdf/29/6/1102/3281404/1102.pdf by guest on 07 April 2023

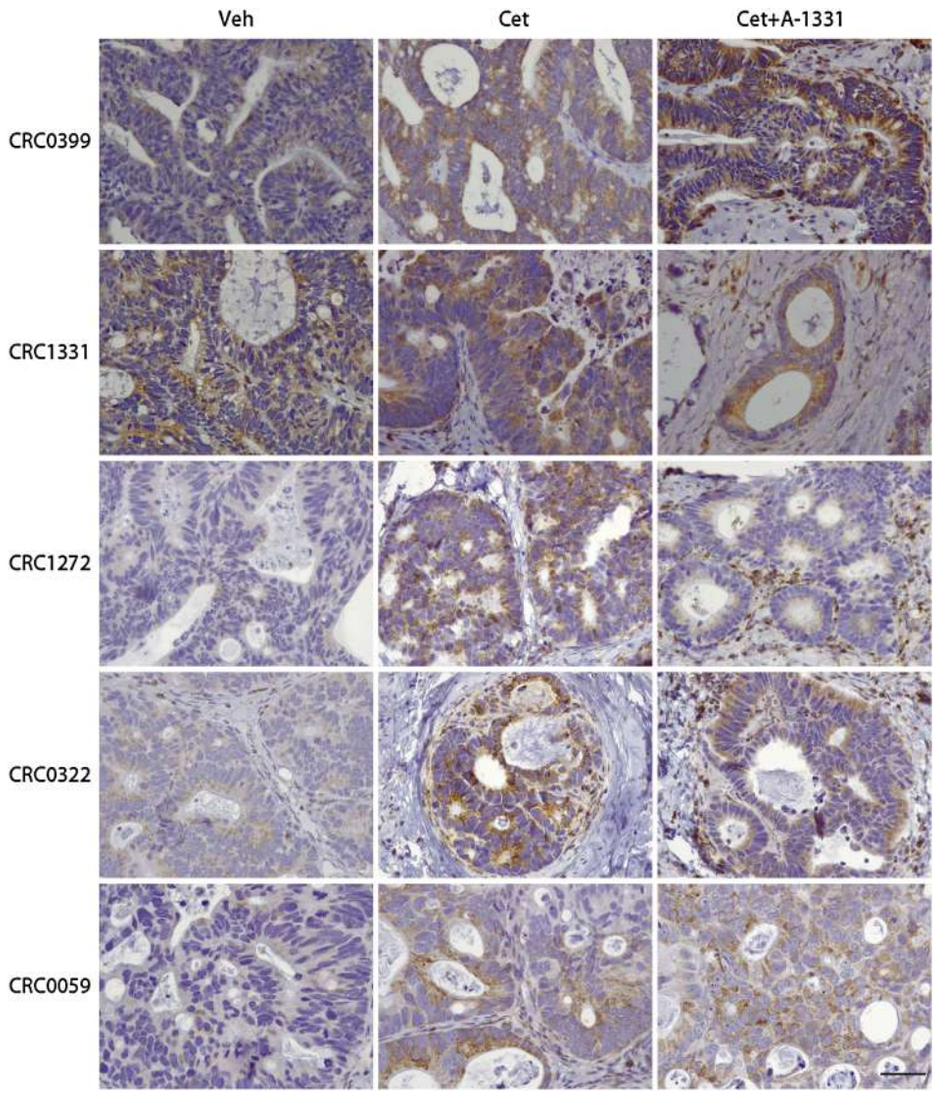

Figure 5.
EGFR inhibition increases BIM protein levels *in vivo*, and high BIM abundance is maintained after concomitant inhibition of BCL-XL. Representative images of BIM immunoreactivity in PDXs after treatment for 5 weeks with cetuximab (20 mg/kg, intraperitoneal injection twice a week) or cetuximab plus A-1331852 (25 mg/kg, oral gavage 5 days a week). At the end of treatment, two to three tumors from 2 to 3 different mice were explanted and subjected to IHC analysis. Veh, vehicle; Cet, cetuximab; A-1331, A-1331852. Scale bar, 50 μm.

signs of apoptosis (10, 25). When considering the spontaneous growth and death dynamics of the tumor mass, regressions induced by a merely cytostatic agent are not unexpected, because therapy may shift the net balance between cell accretion and cell attrition toward one that promotes cell loss without increasing the number of apoptotic cells. However, lack of overt apoptosis prevents tumor obliteration. This is supported by our observation, consolidated after monitoring hundreds of mCRC PDXs exposed to cetuximab (10, 25, 27, 29, 30), that complete responses are exceptional events.

Here we show that treatment of PDX-derived organoids with cetuximab primed cells for death, as assessed by dynamic BH3 profiling, and increased the abundance of the proapoptotic protein BIM. BIM protein levels are negatively regulated by the MAPK pathway through ERK-dependent targeting of BIM to proteasomal degradation (37, 38, 42). BIM protein accumulation in EGFR-inhibited PDXOs is therefore ascribable to cetuximab-mediated inactivation of the MAPK pathway, in line with previous findings (10). BIM induction alone by cetuximab was insufficient to cause apoptosis owing to selective BIM binding to (and inactivation by) BCL-XL. However, disruption of BCL-XL:BIM complexes by navitoclax, with the ensuing release of large amounts of free BIM, precipitated apoptosis. In broad terms, this mechanism is in line with prior evidence whereby inhibition of BCL2 potentiated the efficacy of MEK inhibitors in *BRAF*-mutant melanoma cells (20) and inhibition of MCL1 synergized with HER2 inhibitors or MEK inhibitors in PDXs from *ERBB2*-amplified mammary tumors and in *KRAS*-mutant lung cancer cell lines, respectively (18, 43).

Cetuximab-induced apoptotic priming prompted a specific dependency on BCL-XL, but not on BCL2, which proved to be poorly expressed in mCRC organoids both basally and after cetuximab treatment. Accordingly, inhibition of BCL2 with venetoclax did not unleash apoptosis in the presence of cetuximab. Intriguingly, BCL2 is expressed in normal intestinal stem cells, where it is dispensable for tissue homeostasis and postinjury epithelial regeneration but is essential in the very early phases of adenoma formation following *APC* loss (44). Conversely, BCL-XL is crucial for stem cell survival in late-stage adenomas, and BCL-XL inhibition was found to impair adenoma growth through apoptosis induction (45). Our finding that only concomitant blockade of BCL-XL and EGFR triggered massive cell

Downloaded from http://aacrjournals.org/clincancerres/article-pdf/29/6/1102/3281404/1102.pdf by guest on 07 April 2023

death in mCRC PDXOs suggests that during colorectal cancer progression reliance on BCL-XL is compounded by a newly acquired dependency on EGFR.

The role of MCL1 in EGFR-inhibited mCRC is less clear. An increase in the formation of MCL1:BIM complexes has been documented after exposure of *BRAF*-mutant melanoma cells to the BCL2/BCL-XL inhibitor ABT-737 (20) and in *KRAS*-mutant cells of different origin treated with navitoclax (18, 21). In agreement with these reports, we also found that single-agent navitoclax not only blocked the interaction between BIM and BCL-XL, but also led to some increase in BIM binding to MCL1. Interestingly, adding cetuximab to navitoclax caused a partial loss of MCL1:BIM complexes, which likely increased the availability of free BIM to trigger apoptosis. The ability of cetuximab to partly disrupt MCL1:BIM complexes was manifested only in the presence of navitoclax and in spite of the fact that cetuximab did not affect MCL1 protein expression. Although we did not explore the reasons underlying the modulation of MCL1:BIM stoichiometry by navitoclax and cetuximab, we speculate that the presence of saturating amounts of the BH3 mimetic, coupled with suppression of EGFR signaling, may result in higher expression of an MCL1 endogenous inhibitor that displaces BIM.

The current study offers some unique angles that may facilitate clinical translation. Combination therapies with BH3 mimetics have proven to be effective only in subsets of cancer cell lines from solid tumors. As an example, the combination of a MEK inhibitor with navitoclax demonstrated efficacy in less than 50% of *KRAS*-mutant lung cancer cell lines (18, 21); the remaining half was sensitive to combined blockade of MEK and MCL1, but predictive biomarkers able to distinguish between the two categories are of difficult application in clinical routine (18). Moreover, combinatorial drug screen data with BH3 mimetics have been typically obtained using conventional cell lines (46), which implies a certain degree of attrition and further drug development efforts to achieve clinical application. Here we show that combined inhibition of EGFR and BCL-XL had widespread proapoptotic activity in a panel of 14 cetuximab-sensitive PDXOs. This activity translated into a therapeutic benefit (either more pronounced tumor regressions or longer time to relapse after treatment discontinuation) in the five different PDX models tested. General responsiveness in clinically relevant patient-derived models bodes well for a relatively straightforward translation of these results to the clinical setting, because the biomarker discovery and validation steps can be skipped.

The development of navitoclax faces obstacles due to a high incidence of on-target thrombocytopenia related to the inhibition of BCL-XL in platelets (47). However, combinations of navitoclax and various molecularly targeted drugs continue to be explored in patients, with constantly improving therapeutic indices (17) and initial evidence of clinical benefit; for example, addition of navitoclax to the JAK1/2 inhibitor ruxolitinib improved survival in patients with myelofibrosis who had disease progression or suboptimal response to ruxolitinib monotherapy (48, 49). Furthermore, our observation that cetuximab imparts a unique dependency on BCL-XL provides a rationale for the prospective use of more specific and less toxic BCL-XL inhibitors, such as BCL-XL proteolysis-targeting chimeras that direct BCL-XL to ubiquitin ligases abundant in cancer cells but poorly expressed in platelets (50). The use of selective BCL-XL inhibitors is also expected to avoid the neutropenic effects typical of BCL2 inhibition (39, 41).

Overall, we believe that the combination of cetuximab and BCL-XL inhibitors is mechanistically designed to convert the cytostatic effect of cetuximab into a massive apoptotic outcome in tumors that show biological sensitivity to EGFR inhibition and warrants further investigation as a potential clinical treatment for the vast majority of patients who experience incomplete responses when treated with anti-EGFR antibodies.

Authors' Disclosures

C. Marchiò reports personal fees from Bayer, Roche, AstraZeneca, and Daiichi-Sankyo outside the submitted work. L. Trusolino reports grants from AIRC, Associazione Italiana per la Ricerca sul Cancro, European Union Horizon 2020, and Fondazione Piemontese per la Ricerca sul Cancro-ONLUS during the conduct of the study, as well as grants from Menarini, Merck KGaA, Merus, Pfizer, Servier, and Symphogen outside the submitted work. A. Bertotti reports grants from AIRC (Italian Association for Cancer Research) during the conduct of the study, as well as grants from AIRC (Italian Association For Cancer Research) and ERC outside the submitted work. No disclosures were reported by the other authors.

Authors' Contributions

S.M. Leto: Conceptualization, data curation, formal analysis, validation, investigation, visualization, methodology, writing–original draft. **M. Ferri:** Formal analysis, investigation, methodology. **F. Sassi:** Formal analysis, investigation, visualization, methodology. **E.R. Zanella:** Data curation, formal analysis, visualization, methodology. **F. Cottino:** Investigation. **V. Vurchio:** Investigation. **I. Catalano:** Investigation. **A. Ferrero:** Resources, methodology. **C.C. Zingaretti:** Resources, methodology. **C. Marchiò:** Investigation, visualization, methodology. **E. Grassi:** Data curation, software, formal analysis, visualization, methodology. **L. Trusolino:** Conceptualization, supervision, funding acquisition, writing–original draft, writing–review and editing. **A. Bertotti:** Conceptualization, data curation, formal analysis, supervision, funding acquisition, writing–review and editing.

Acknowledgments

We acknowledge Merck KGaA for providing cetuximab. We thank Joan Montero and Anthony Letai for suggestions; Marco Avolio, Francesco Galimi, Barbara Lupo, Marika Pinnelli, Carmelo Gabriele Pizzino, and Marco Viviani for discussion; Maurizio Degiuli, Alfredo Mellano, Mauro Papotti, Gianluca Paraluppi, and Serena Perotti for sample acquisition; Barbara Martinoglio for support with real-time PCR; Massenzio Fornasier and Arianna Russo for veterinary assistance; Fabrizio Maina for animal husbandry; Raffaella Albano, Stefania Giove, Lara Fontani, and Laura Palmas for technical assistance; and Daniela Gramaglia and Mauro Paschetta for secretarial assistance. This work has been supported by AIRC, Associazione Italiana per la Ricerca sul Cancro, Investigator Grants 20697 (to A. Bertotti) and 22802 (to L. Trusolino); AIRC 5×1000 grant 21091 (to A. Bertotti and L. Trusolino); AIRC/CRUK/FC AECC Accelerator Award 22795 (to L. Trusolino); European Research Council Consolidator Grant 724748 BEAT (to A. Bertotti); H2020 grant agreement no. 754923 COLOSSUS (to L. Trusolino); H2020 INFRAIA grant agreement no. 731105 EDIReX (to A. Bertotti); and Fondazione Piemontese per la Ricerca sul Cancro-ONLUS, 5×1000 Ministero della Salute 2016 (to L. Trusolino).

The publication costs of this article were defrayed in part by the payment of publication fees. Therefore, and solely to indicate this fact, this article is hereby marked "advertisement" in accordance with 18 USC section 1734.

Note

Supplementary data for this article are available at Clinical Cancer Research Online (http://clincancerres.aacrjournals.org/).

Received August 16, 2022; revised December 2, 2022; accepted January 6, 2023; published first January 9, 2023.

References

1. Sung H, Ferlay J, Siegel RL, Laversanne M, Soerjomataram I, Jemal A, et al. Global cancer statistics 2020: GLOBOCAN estimates of incidence and mortality worldwide for 36 cancers in 185 countries. CA Cancer J Clin 2021;71:209–49.

Downloaded from http://aacrjournals.org/clincancerres/article-pdf/29/6/1102/3281404/1102.pdf by guest on 07 April 2023

2. Biller LH, Schrag D. Diagnosis and treatment of metastatic colorectal cancer: a review. JAMA 2021;325:669–85.
3. Van Cutsem E, Lenz HJ, Köhne CH, Heinemann V, Tejpar S, Melezínek I, et al. Fluorouracil, leucovorin, and irinotecan plus cetuximab treatment and RAS mutations in colorectal cancer. J Clin Oncol 2015;33:692–700.
4. Fornasier G, Francescon S, Baldo P. An update of efficacy and safety of cetuximab in metastatic colorectal cancer: a narrative review. Adv Ther 2018;35:1497–509.
5. Douillard JY, Oliner KS, Siena S, Tabernero J, Burkes R, Barugel M, et al. Panitumumab-FOLFOX4 treatment and RAS mutations in colorectal cancer. N Engl J Med 2013;369:1023–34.
6. Bivona TG, Doebele RC. A framework for understanding and targeting residual disease in oncogene-driven solid cancers. Nat Med 2016;22:472–8.
7. Piessevaux H, Buyse M, Schlichting M, Van Cutsem E, Bokemeyer C, Heeger S, et al. Use of early tumor shrinkage to predict long-term outcome in metastatic colorectal cancer treated with cetuximab. J Clin Oncol 2013;31:3764–75.
8. Douillard JY, Siena S, Peeters M, Koukakis R, Terwey JH, Tabernero J. Impact of early tumour shrinkage and resection on outcomes in patients with wild-type RAS metastatic colorectal cancer. Eur J Cancer 2015;51:1231–42.
9. Cabanos HF, Hata AN. Emerging insights into targeted therapy-tolerant persister cells in cancer. Cancers 2021;13:2666.
10. Lupo B, Sassi F, Pinnelli M, Galimi F, Zanella ER, Vurchio V, et al. Colorectal cancer residual disease at maximal response to EGFR blockade displays a druggable paneth cell-like phenotype. Sci Transl Med 2020;12:eaax8313.
11. Hata AN, Niederst MJ, Archibald HL, Gomez-Caraballo M, Siddiqui FM, Mulvey HE, et al. Tumor cells can follow distinct evolutionary paths to become resistant to epidermal growth factor receptor inhibition. Nat Med 2016;22:262–9.
12. Singh R, Letai A, Sarosiek K. Regulation of apoptosis in health and disease: the balancing act of BCL-2 family proteins. Nat Rev Mol Cell Biol 2019;20:175–93.
13. Hata AN, Engelman JA, Faber AC. The BCL2 family: key mediators of the apoptotic response to targeted anticancer therapeutics. Cancer Discov 2015;5:475–87.
14. Diepstraten ST, Anderson MA, Czabotar PE, Lessene G, Strasser A, Kelly GL. The manipulation of apoptosis for cancer therapy using BH3-mimetic drugs. Nat Rev Cancer 2022;22:45–64.
15. Roberts AW, Davids MS, Pagel JM, Kahl BS, Puvvada SD, Gerecitano JF, et al. Targeting BCL2 with venetoclax in relapsed chronic lymphocytic leukemia. N Engl J Med 2016;374:311–22.
16. DiNardo CD, Jonas BA, Pullarkat V, Thirman MJ, Garcia JS, Wei AH, et al. Azacitidine and venetoclax in previously untreated acute myeloid leukemia. N Engl J Med 2020;383:617–29.
17. Carneiro BA, El-Deiry WS. Targeting apoptosis in cancer therapy. Nat Rev Clin Oncol 2020;17:395–417.
18. Nangia V, Siddiqui FM, Caenepeel S, Timonina D, Bilton SJ, Phan N, et al. Exploiting MCL1 dependency with combination MEK + MCL1 inhibitors leads to induction of apoptosis and tumor regression in KRAS-mutant non–small cell lung cancer. Cancer Discov 2018;8:1598–613.
19. Cragg MS, Kuroda J, Puthalakath H, Huang DC, Strasser A. Gefitinib-induced killing of NSCLC cell lines expressing mutant EGFR requires BIM and can be enhanced by BH3 mimetics. PLoS Med 2007;4:1681–9.
20. Cragg MS, Jansen ES, Cook M, Harris C, Strasser A, Scott CL. Treatment of B-RAF mutant human tumor cells with a MEK inhibitor requires Bim and is enhanced by a BH3 mimetic. J Clin Invest 2008;118:3651–9.
21. Corcoran RB, Cheng KA, Hata AN, Faber AC, Ebi H, Coffee EM, et al. Synthetic lethal interaction of combined BCL-XL and MEK inhibition promotes tumor regressions in KRAS mutant cancer models. Cancer Cell 2013;23:121–8.
22. Faber AC, Farago AF, Costa C, Dastur A, Gomez-Caraballo M, Robbins R, et al. Assessment of ABT-263 activity across a cancer cell line collection leads to a potent combination therapy for small-cell lung cancer. Proc Natl Acad Sci U S A 2015;112:E1288–96.
23. Sale MJ, Minihane E, Monks NR, Gilley R, Richards FM, Schifferli KP, et al. Targeting melanoma's MCL1 bias unleashes the apoptotic potential of BRAF and ERK1/2 pathway inhibitors. Nat Commun 2019;10:5167.
24. Sale MJ, Cook SJ. The BH3 mimetic ABT-263 synergizes with the MEK1/2 inhibitor selumetinib/AZD6244 to promote BIM-dependent tumour cell death and inhibit acquired resistance. Biochem J 2013;450:285–94.
25. Zanella ER, Galimi F, Sassi F, Migliardi G, Cottino F, Leto SM, et al. IGF2 is an actionable target that identifies a distinct subpopulation of colorectal cancer patients with marginal response to anti-EGFR therapies. Sci Transl Med 2015;7:272ra12.
26. Ryan J, Montero J, Rocco J, Letai A. iBH3: simple, fixable BH3 profiling to determine apoptotic priming in primary tissue by flow cytometry. Biol Chem 2016;397:671–8.
27. Bertotti A, Migliardi G, Galimi F, Sassi F, Torti D, Isella C, et al. A molecularly annotated platform of patient-derived xenografts ("xenopatients") identifies HER2 as an effective therapeutic target in cetuximab-resistant colorectal cancer. Cancer Discov 2011;1:508–23.
28. Baralis E, Bertotti A, Fiori A, Grand A. LAS: a software platform to support oncological data management. J Med Syst 2012;36:S81–90.
29. Bertotti A, Papp E, Jones S, Adleff V, Anagnostou V, Lupo B, et al. The genomic landscape of response to EGFR blockade in colorectal cancer. Nature 2015;526:263–7.
30. Isella C, Brundu F, Bellomo SE, Galimi F, Zanella E, Porporato R, et al. Selective analysis of cancer-cell intrinsic transcriptional traits defines novel clinically relevant subtypes of colorectal cancer. Nat Commun 2017;8:15107.
31. Schütte M, Risch T, Abdavi-Azar N, Boehnke K, Schumacher D, Keil M, et al. Molecular dissection of colorectal cancer in pre-clinical models identifies biomarkers predicting sensitivity to EGFR inhibitors. Nat Commun 2017;8:14262.
32. Vlachogiannis G, Hedayat S, Vatsiou A, Jamin Y, Fernández-Mateos J, Khan K, et al. Patient-derived organoids model treatment response of metastatic gastrointestinal cancers. Science 2018;359:920–6.
33. Guillen KP, Fujita M, Butterfield AJ, Scherer SD, Bailey MH, Chu Z, et al. A human breast cancer-derived xenograft and organoid platform for drug discovery and precision oncology. Nat Cancer 2022;3:232–50.
34. Montero J, Sarosiek KA, DeAngelo JD, Maertens O, Ryan J, Ercan D, et al. Drug-induced death signaling strategy rapidly predicts cancer response to chemotherapy. Cell 2015;160:977–89.
35. Daniels VW, Zoeller JJ, van Gastel N, McQueeney KE, Parvin S, Potter DS, et al. Metabolic perturbations sensitize triple-negative breast cancers to apoptosis induced by BH3 mimetics. Sci Signal 2021;14:eabc7405.
36. Senichkin VV, Streletskaia AY, Gorbunova AS, Zhivotovsky B, Kopeina GS. Saga of Mcl-1: regulation from transcription to degradation. Cell Death Differ 2020;27:405–19.
37. Luciano F, Jacquel A, Colosetti P, Herrant M, Cagnol S, Pages G, et al. Phosphorylation of Bim-EL by Erk1/2 on serine 69 promotes its degradation via the proteasome pathway and regulates its proapoptotic function. Oncogene 2003;22:6785–93.
38. Meng J, Fang B, Liao Y, Chresta CM, Smith PD, Roth JA. Apoptosis induction by MEK inhibition in human lung cancer cells is mediated by Bim. PLoS One 2010;5:e13026.
39. Leverson JD, Phillips DC, Mitten MJ, Boghaert ER, Diaz D, Tahir SK, et al. Exploiting selective BCL-2 family inhibitors to dissect cell survival dependencies and define improved strategies for cancer therapy. Sci Transl Med 2015;7:279ra40.
40. Corona SP, Walker F, Weinstock J, Lessene G, Faux M, Burgess AW. Dual drug targeting to kill colon cancers. Cancer Med 2022;11:2612–26.
41. Wang L, Doherty GA, Judd AS, Tao ZF, Hansen TM, Frey RR, et al. Discovery of A-1331852, a first-in-class, potent, and orally-bioavailable BCL-X. ACS Med Chem Lett 2020;11:1829–36.
42. Faber AC, Li D, Song Y, Liang MC, Yeap BY, Bronson RT, et al. Differential induction of apoptosis in HER2 and EGFR addicted cancers following PI3K inhibition. Proc Natl Acad Sci U S A 2009;106:19503–8.
43. Merino D, Whittle JR, Vaillant F, Serrano A, Gong JN, Giner G, et al. Synergistic action of the MCL-1 inhibitor S63845 with current therapies in preclinical models of triple-negative and HER2-amplified breast cancer. Sci Transl Med 2017;9:eaam7049.
44. van der Heijden M, Zimberlin CD, Nicholson AM, Colak S, Kemp R, Meijer SL, et al. Bcl-2 is a critical mediator of intestinal transformation. Nat Commun 2016;7:10916.
45. Ramesh P, Lannagan TRM, Jackstadt R, Atencia Taboada L, Lansu N, Wirapati P, et al. BCL-XL is crucial for progression through the adenoma-to-carcinoma sequence of colorectal cancer. Cell Death Differ 2021;28:3282–96.

Downloaded from http://aacrjournals.org/clincancerres/article-pdf/29/6/1102/3281404/1102.pdf by guest on 07 April 2023

46. Jaaks P, Coker EA, Vis DJ, Edwards O, Carpenter EF, Leto SM, et al. Effective drug combinations in breast, colon and pancreatic cancer cells. Nature 2022;603:166–73.
47. Roberts AW, Seymour JF, Brown JR, Wierda WG, Kipps TJ, Khaw SL, et al. Substantial susceptibility of chronic lymphocytic leukemia to BCL2 inhibition: results of a phase I study of navitoclax in patients with relapsed or refractory disease. J Clin Oncol 2012;30:488–96.
48. Pemmaraju N, Garcia JS, Potluri J, Harb JG, Sun Y, Jung P, et al. Addition of navitoclax to ongoing ruxolitinib treatment in patients with myelofibrosis (REFINE): a *post-hoc* analysis of molecular biomarkers in a phase 2 study. Lancet Haematol 2022;9:e434–e44.
49. Harrison CN, Garcia JS, Somervaille TCP, Foran JM, Verstovsek S, Jamieson C, et al. Addition of navitoclax to ongoing ruxolitinib therapy for patients with myelofibrosis with progression or suboptimal response: phase II safety and efficacy. J Clin Oncol 2022;40:1671–80.
50. Khan S, Zhang X, Lv D, Zhang Q, He Y, Zhang P, et al. A selective BCL-XL PROTAC degrader achieves safe and potent antitumor activity. Nat Med 2019;25:1938–47.

Downloaded from http://aacrjournals.org/clincancerres/article-pdf/29/6/1102/3281404/1102.pdf by guest on 07 April 2023